IMAGE SEGMENTATION TECHNIQUES FOR STEM CELL TRACKING

Ching-Fen Jiang and Ka-Pei Tsai

Department of Biomedical Engineering,
I-Shou University, Kaohsiung, Taiwan, R.O.C.

ABSTRACT

To grow stem cells in vitro is an important task in regenerative medicine. Cell motility that can be derived by cell tracking is a useful index to evaluate the viability and stemness of stem cells. The precision of cell tracking is highly dependent on correct detection of the cell centroids, which are usually determined by cell segmentation process. In this study, a cell segmentation method combining double-thresholding and disk-based reconstruction is proposed to solve the problems arising from shape deformation and uneven illumination during cell culture. The qualitative and quantitative comparisons show that the proposed segmentation method increases accuracy in detection the cell centroid.

Index Terms— Stem cell, cell tracking, segmentation, circular Hough transform

1. INTRODUCTION

Stem cell can differentiate into diverse specialized cells and with this mechanism the human body can be repaired and replenished. It brings conventional medicine into a new turning point and therefore become very important in modern medicine. Recently, regenerative medicine focuses on growing stem cell in vitro, then implanting them into human body to help self-recovery [1-3]. However, the big challenge occurs while culturing stem cells in vitro, because their viability and stemness are subjected to change with microenvironment. How to assess these changes correctly is a big issue for the bases to develop a suitable microenvironment for cell culture.

Stem cell motility is a useful index to evaluate the viability and stemness of stem cells. Currently, the most widely used method to observe stem cell activity qualitatively is visual inspection through a microscope. However, manually performing quantitative assessments of cell behavior is time consuming and prone to human error. A computer-aided analysis tool is thus required for an effective analysis of the stem cell motility via cell tracking.

In the literature, several cell tracking methods have been reported, including those using the Bayesian probabilistic to predict the path [4], regarding the cell motion as optical flow [5], and geometric similarity-based tracking [6-8]. Despite different cell-tracking algorithms, cell segmentation is usually the first step to define the location of the cell in a series of video frames, based on that the variation in the locations of a specific cell between the adjacent frames defines the cell motility. Therefore, the precision of cell tracking is under the influence of correctness of cell segmentation.

The degree of complexity of cell segmentation depends on cell morphology and cell imaging modalities. For fluorescence microscopy, the disk-like cells can be regards as a dynamic light particle; therefore, thresholding methods may be sufficient to detect the cell [4]. For light microscopy, cells with irregular shape require more sophisticated methods to recognize, such as wavelet [9], watershed [10] and deformable model [6].

However, neither of the above methods alone fulfills our needs to segment the stem cell. This is because the shape of the stem cell is subject to change during cell culture as shown in Fig. 1. In addition, the inhomogeneous illumination induced by uneven reflection from the cultural medium increases the difficulty in cell segmentation using single threshold. Therefore, this study aims to develop an efficient cell segmentation scheme to solve the aforementioned problems.

2. MATERIAL AND METHODS

2.1. Cell Image Acquisition

In this study, we focused on mesenchymal stem cells that exist inside bone marrow, the umbilical cord blood of newborns, and the peripheral blood of adults. Mesenchymal stem cells have a great capacity for self-renewal while maintaining their multipotency. This property increases its research value regarding cell therapy, tissue construction, and regenerative medicine. In addition, compared to other adult stem cells, mesenchymal stem cells have better self-renewal and proliferation abilities. Subsequently, their implementation in the repair of damaged tissue and organs has increased in recent years, especially in applied clinical research.

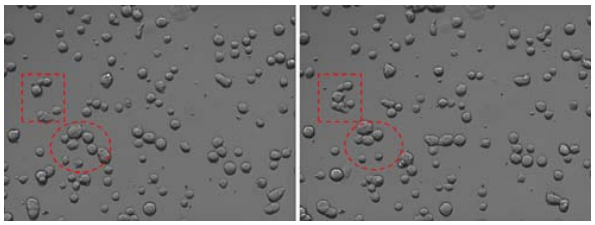

(a) (b)

Fig.1 Two successive image frames show changes in the cell shapes highlighted in the square and circle zones.

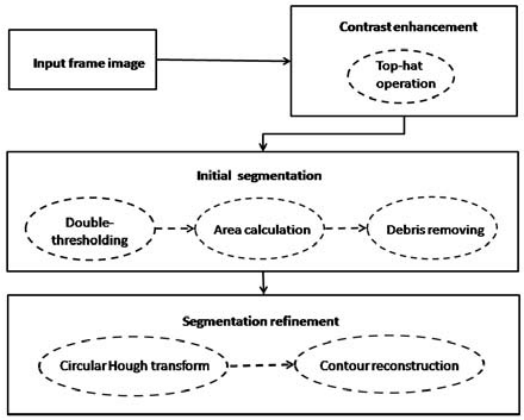

Fig. 2 Cell segmentation scheme.

The cell video was recorded by the ASTECR® CCM-1.4XZY/CO2 system with a CCD camera embedded on a time lapse microscope.

2.2. Image Segmentation

As mentioned previously in Introduction, there are two problems in our segmentation tasks. First, the jelly-like culture medium causes uneven reflectance on the image background, leading to a false cell detection using intensity thresholding method. Second, the cell deformation during aggregation process increases complexity in cell segmentation. In addition, these problems were majorly found with single cells.

To solve these two problems, a systematic segmentation approach was developed. It contains three phases:

1) *Illumination correction*

The top-hat method [11] was applied to correct images with non-uniformities in background luminance. The formula is shown below:

$$\mathrm{I} = \mathrm{A}' - (\mathrm{A}' \circ B) \tag{1}$$

A represents the original image, and A' is with inversed luminosity. B represents the template with a size of half the cell. ' ∘ ' denotes the morphological opening operation, and **I** represents the image after applying the Top-hat method.

2) *Initial Segmentation*

A statistic-based auto-thresholding method was used for initial segmentation [12, 13]. This algorithm automatically and objectively determines intensity threshold value(s) within an image histogram that maximize(s) the variability between the resulting pixel classes; thus, it separates the image into clusters with similar intensities. Because the cell images showed blurred contours due to smooth intensity changes, according to our experiences, for these kind of images three-clustering process renders better segmentation results than two clustering does; therefore, the original one-threshold algorithm was modified into two thresholds to classify the image into three clusters.

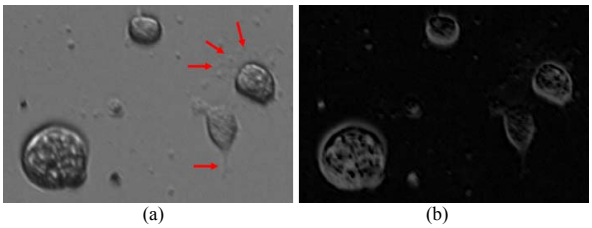

(a) (b)

Fig.3 (a) The uneven background, especially on the regions close to cell (pointed by arrows) increase the difficulty in cell segmentation. (b) The background is unified by the Top-hat operation.

The algorithm derives the optimal thresholds k_1^* and k_2^* to separate objects by maximizing the between-class variance δ_B^2.

$$\delta_B^2(k_1,k_2) = w_0(\mu_0-\mu_T)^2 + w_1(\mu_1-\mu_T)^2 + w_2(\mu_2-\mu_T)^2 \tag{2}$$

$$\delta_B^2(k_1^*,k_2^*) = \max_{1\le k_1<k_2<L} \delta_B^2(k_1,k_2) \tag{3}$$

where w_0, w_1 and w_2 are the probabilities of the three non-overlapping classes in the images, μ_0 , μ_1 and μ_2 are their mean gray values, and μ_T is the mean gray value of the entire image. An optimal set of thresholds k_1^* and k_2^* can be selected by maximizing δ_B^2 through an iterative search process. The lower value of threshold was used to extract the cellular area.

After thresholding, the area of each isolated object was derived from the binary images. Some debris, which was not belonging to stem cells, can be detected by the area constraint. An area threshold A_{th} of an isolated object was used to remove segmentation debris. An isolated object with the area smaller than A_{th} was regarded as debris. The value of A_{th} was determined empirically.

3) *Segmentation refinement*

In some image frames, we found that many cells only preserved lower half part after initial segmentation. It could be due to a specific light emission direction that made the part of the contour facing the light brighter than those on the back side of the light. We called this phenomenon a shadow

effect. Even though Top-hat operation solved the problem of uneven background luminance, the shadow problem remained unsolved. This problem was found frequently associated with singles cells and would cause incomplete segmentation. Fig. 4(a) demonstrates this shadow effect where the upper half contours of the cells are brighter than the lower half contours; therefore, the brighter part tends to be classified as the background and to be removed. Finally, the cells with the shadow effect only remain a moon-wane shape as those cells labeled in Fig. 4(b). Because the phenomenon only occurred before cell aggregation, we used two criteria to detect those fragmented contour for following process. First, the area of a single segmented entity should be smaller than the area of a normal cell. Second, the shape index, *SI*, should be greater than 1. The *SI* was defined as the ratio of the measured contour length (p) to the derived contour length (p'). The closer the irregular degree value was to 1, the closer the cell was to being completely circle.

$$SI = p/p', \quad \text{where } p' = 2\pi\sqrt{\frac{Area}{\pi}} \tag{4}$$

Following that, to fill the missing part of the fragmented contour, we adopted the Circular Hough transform (CHT) [14] to gain the initial contour points P_i and used these points to search for the optimal contour for final contour reconstruction. The basis of the CHT is to map a circle with a certain range of radii (R) on each edge point and count the intersection of those circles. The optimal circle is determined by searching for the R with the maximal intersection. However, the cell shape in the images was not exactly a circle. Therefore, the edge points above the center of the circle where the missing contour occurred were used as the starting points P_i to search for the real contour points with maximal gradients (Fig. 5). The search direction was determined by the starting points and the center of the circle. The search range was pre-defined as a segment of the line centered at the point P_i. The final contour was reconstructed by interpolating these contour edges using cubic spline.

3. RESULTS AND DISCUSSIONS

The results of each processing stage are given in following figures for further discussions. Fig. 6 demonstrates comparison of segmentation effect with different approaches to the original image of Fig.3 (a). A cell in the red square in Fig. 6(a) is missing while applying conventional single-thresholding method. Lower part of the cell in Fig. 6(b) is detected by double thresholding even without applying Top-hat enhancement. Double thresholding followed by the Top-hat operation yields a more complete cell shape in Fig.6(c).

Fig. 7 shows the cell contour reconstructed through the CHT to fill up the incomplete contour of the cells with shadowing effect. As mentioned previously in Section 2.2, the shadow effect seen in Fig. 4(a) results in fragmented cell using double-thresholding method as shown in Fig. 4(b). The disks derived by the CHT are placed over the contours of the detected fragmented cell in Fig. 7 (a). They were used as the initial contours to search for the real contours. A typical case given in Fig. 7 (b) was used as an example to illustrate the mid- and final result at each stage.

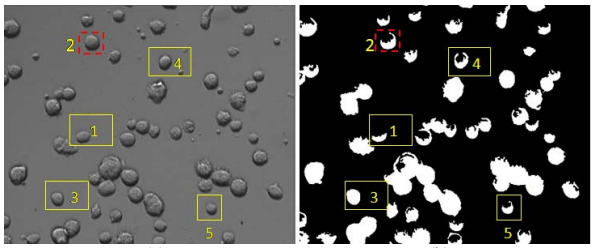

(a) (b)

Fig.4 (a) Illustration of the shadow effect. (b) The cells affected by this effect become fragmented after thresholding segmentation. The five labeled cells are used to assess the accuracy of centroid detection in Table 1.

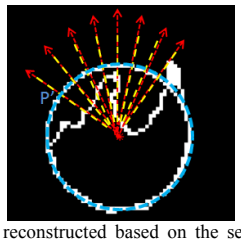

Fig.5 The contour is reconstructed based on the search for the maximal gradient along the radiant path (indicated by red arrows) from the center of the disk (indicated by blue dashed line) obtained by the CHT.

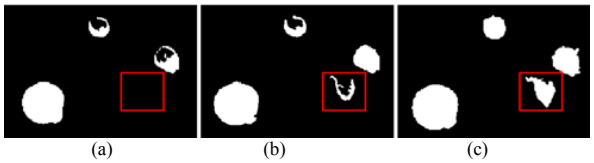

(a) (b) (c)

Fig.6 Segmentation results of Fig. 3(a). Results obtained by (a) using conventional single-thresholding after Top-hat enhancement; (b) using double-threshold without Top-hat enhancement; and (c) using double-threshold after Top-hat enhancement.

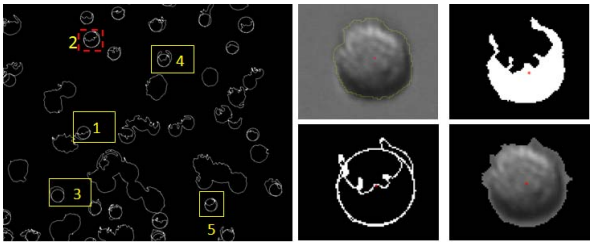

(a) (b)

Fig.7 (a) The disks derived by the CHT are overlaid on the contours of the detected fragmented cells from initial segmentation. Five cells are labeled herein. The upper-left panel in (b) is the cell contour of cell number 2 (in red dashed square) determined by visual inspection. The upper-right is the initial segmentation. The lower-left is the contour overlaid by the CHT disk and the lower-right is the final result after contour reconstruction.

The centroid for each mid-stage contour is labeled on the image. As the centroid of the cell is usually used as the marker to track the cell path, precise detection of the centroid location in the image frame is thus essential and of a great influence on the cell tracking accuracy. As the incomplete cell segmentation affected the centroid detection much more in a single cell than that on a cell cluster, we used five single cells labeled with a sequence of numbers in Figs. 4 and 6 to derive the distance between the derived centroid and the real centroid of the original image. The quantitative result is given in Table 1 where shows that the centroids of all the final segmented cells are the closest to the real centroids in comparison with the mid-results. Therefore, these results suggest that the proposed cell segmentation scheme has effectively targeted the cell location.

4. CONCLUSION

Cell tracking is an essential work to evaluate the viability of stem cell. The precision of cell tracking is highly dependent on correct detection of the cell centroids, which are usually determined by cell segmentation process. Even though several cell segmentation methods have been reported in the literature, none of them meet our special needs to solve the problems arisen from cell deformation and uneven illumination during cell culture. To segment cells with complex background, thresholding methods are usually insufficient; therefore, several methods based on sophisticated iteration process to find the optimal contours were proposed. However, they are time-consuming. In this study, we took a different path from the prior studies by using thresholding approach associated with morphological contrast enhancement for initial segmentation. For those incomplete segmented cell, we then used a disk-based model of the Circular Hough transform to recover those cells. The comparison of the difference between the real and the detected centroids of five cells shows that the proposed method increased the accuracy in centroid detection.

Table 1
The distance of the detected centroid to the real centroid of the each cell

label / method	1	2	3	4	5	mean ±std
initial result	11.2	9.8	9.5	4.5	4.2	7.8±3.3
CHT disk	5.1	4.5	5.4	2.3	3.2	4.1±1.3
reconstructed results	2.8	3.6	3.6	1	2.2	2.6±1.1

unit: pixel

ACKNOWLEDGEMENT

This study is supported by the grant from the National Science Council of Taiwan (NSC 101-2221-E-214-009-MY3). The authors acknowledge the images provided by Prof. Shan-Hui Hsu in Institute of Polymer Science and Engineering, National Taiwan University, Taiwan.

REFERENCES

[1] S. Hsu, T. B. Huang, S. J. Cheng, S. Y. Weng, C. L. Tsai, C. S. Tseng, D. C. Chen, T. Y. Liu, K. Y. Fu, and B. L. Yen, "Chondrogenesis from human placenta-derived mesenchymal stem cells in three-dimensional scaffolds for cartilage tissue engineering," *Tissue Engineering Part A,* vol. 17, pp. 1549-1560, 2011.

[2] S. Hsu, S. H. Chan, C. M. Chiang, C. Chi-Chang Chen, and C. F. Jiang, "Peripheral nerve regeneration using a microporous polylactic acid asymmetric conduit in a rabbit long-gap sciatic nerve transection model," *Biomaterials,* 2011.

[3] J. C. Chang, S. Hsu, and D. C. Chen, "The promotion of chondrogenesis in adipose-derived adult stem cells by an RGD-chimeric protein in 3D alginate culture," *Biomaterials,* vol. 30, pp. 6265-6275, 2009.

[4] N. N. Kachouie, P. Fieguth, J. Ramunas, and E. Jervis, "Probabilistic model-based cell tracking," *International Journal of Biomedical Imaging,* vol. 2006, pp. 1-10, 2006.

[5] G. A. Dunn and G. E. Jones, "Cell motility under the microscope: Vorsprung durch Technik," *Nature Reviews Molecular Cell Biology,* vol. 5, pp. 667-672, 2004.

[6] C. Zimmer, E. Labruyere, V. Meas-Yedid, N. Guillen, and J. C. Olivo-Marin, "Segmentation and tracking of migrating cells in videomicroscopy with parametric active contours: a tool for cell-based drug testing," *IEEE Trans. Med. Imag.,* vol. 21, pp. 1212-1221, 2002.

[7] N. Kachouie, P. Fieguth, J. Ramunas, and E. Jervis, "A model-based hematopoietic stem cell tracker," *Image Analysis and Recognition,* pp. 861-868, 2005.

[8] O. Debeir, P. Van Ham, R. Kiss, and C. Decaestecker, "Tracking of migrating cells under phase-contrast video microscopy with combined mean-shift processes," *IEEE Trans. Med. Imag.,* vol. 24, pp. 697-711, 2005.

[9] D. Padfield, J. Rittscher, and B. Roysam, "Coupled minimum-cost flow cell tracking," pp. 374-385, 2009.

[10] X. Chen, X. Zhou, and S. T. C. Wong, "Automated segmentation, classification, and tracking of cancer cell nuclei in time-lapse microscopy," *IEEE Trans. Biomed. Eng.,* vol. 53, pp. 762-766, 2006.

[11] M. A. A. Dewan, M. O. Ahmad, and M. N. S. Swamy, "Tracking Biological Cells in Time-Lapse Microscopy: An Adaptive Technique Combining Motion and Topological Features," *IEEE Trans. Biomed. Eng.,* vol. 58, pp. 1637-1647, Jun 2011.

[12] P. S. Liao, T. S. Chen and P. C. Chung, "A Fast Algorithm for Multilevel Thresholding," *J. Inf. Sci. Eng.*, vol. 17, no. 5. pp. 713–727, 2001.

[13] C.F. Jiang, T.C. Lu, S.P. Sun, "Interactive Image Registration Tool for Positioning Verification in Head and Neck Radiotherapy," *Comput. Biol. Med.*, vol. 38, no. 1, pp. 90-100, 2008.01

[14] A. Flores-Mendez and A. Suarez-Cervantes, "Circular degree Hough transform," *Progress in Pattern Recognition, Image Analysis, Computer Vision, and Applications,* pp. 287-294, 2009.